Scalable modeling and comparison for spiral inductors using enhanced 1-π and 2-π topologies*

Zou Huanhuan(邹欢欢)†, Sun Lingling(孙玲玲), Wen Jincai(文进才), and Liu Jun(刘军)

(Key Laboratory of RF Circuits and Systems, Ministry of Education, Hangzhou Dianzi University, Hangzhou 310018, China)

Abstract: Two different scalable models developed based on enhanced 1-π and 2-π topologies are presented for on-chip spiral inductor modeling. All elements used in the two topologies for accurately predicting the characteristics of spiral inductors at radio frequencies are constructed in geometry-dependent equations for scalable modeling. Then a comparison between the 1-π and 2-π scalable models is made from the following aspects: the complexity of equivalent circuit models and parameter-extraction procedures, scalable rules and the accuracy of scalable models. The two scalable models are further verified by the excellent match between the measured and simulated results on extracted parameters up to self-resonant frequency (SRF) for a set of spiral inductors with different L, R and N, which are fabricated by employing 0.18-μm 1P6M RF CMOS technology.

Key words: RF-CMOS; on-chip spiral inductor; scalable model; 1-π; 2-π
DOI: 10.1088/1674-4926/31/5/055011 **EEACC:** 1110; 2140; 2560

1. Introduction

The RF performance of CMOS technology has been improved constantly over the past years[1−4]. CMOS technology has now become a popular choice for realizing RF application. An important issue for RF devices is the availability of compact RF models to accurately predict the RF characteristics at high frequencies. As important devices, on-chip spiral inductors are widely used in RF circuits, such as low-noise amplifiers (LNAs), power amplifiers (PAs), mixers and voltage-controlled oscillators (VCOs). The scalability and the accuracy of the equivalent circuit models for on-chip inductor modeling are of the utmost importance for CMOS mixed-signal/RF SoC designs.

Many papers have reported equivalent circuit models of on-chip spiral inductors, such as the 9-element 1-π model[5], modified 1-π model[6, 7], 2-π model[8−10] and T model[11, 12]. As the distributed effects and the higher order loss effects are not properly considered in the 9-element 1-π model, other equivalent circuit models such as the modified 1-π, 2-π and T models are developed for RF spiral inductors, representing the skin and proximity effects in metallization and eddy-current loss caused by the silicon substrate[6−12]. Compared to the 1-π model, T models can be used accurately at a higher frequency range, but they always suffer from difficulties in accurately extracting all the parameter values as well as poor scalability of the parameters.

The modified 1-π model proposed in Ref. [6] models lateral substrate coupling by a substrate inductor L_{sub} (magnetically coupled to L_s) and series resistor R_{sub}. As the regulation of mutual inductance is indistinct in the real world, the introduction of the mutual inductance between L_s and L_{sub} leads to difficulties in parameter extraction and determination of the scalabilities from the extracted values of L_s and L_{sub}; thus, one has to depend on data fitting. Furthermore, the accuracy of this modified 1-π scalable model has not been verified by a series of inductors with different geometries. In the enhanced 1-π model proposed in Ref. [7], a parallel network ($R_{sub}//C_{sub}$) is utilized to model the lateral substrate coupling, which facilitates the procedure of parameter extraction and improves the scalability. The non-symmetrical inductor feature is considered in Ref. [8] by using an asymmetric 2-π topology, but the determination of the partition factor is ambiguous. Transformer loops (magnetically coupled to L_{dc}) are utilized in the 2-π model proposed in Ref. [9], representing the frequency-dependent series loss accurately and making the model wideband. However, it does not achieve scalability. A 2-π scalable model is established in Ref. [10]. A set of complicated functions are utilized to calculate C_{ox}, C_{si} and C_p, making the parameter-extraction procedure and scalable rules intricate.

For mixed-signal/RF SoC design, a scalable model of inductors is useful. A scalable model with high accuracy facilitates the procedure of circuit design and improves the performance of circuits. However, there is little detailed work about scalable models of inductors as well as the comparison between 1-π and 2-π scalable models. In this paper, an enhanced 1-π scalable model is established. This topology was first proposed in Ref. [7]. Two different parameter-extraction methodologies for fixed inductors are developed in Refs. [13, 14]. However, a scalable model based on this enhanced 1-π topology has not been reported. For broad applications of 2-π models and the lack of simple 2-π scalable models, a 2-π scalable model is also set up in this paper. All the equivalent-circuit elements in the two scalable models are related to the geometric parameters through a set of formulas which are composed of polynomials based on physical insights. Then a comparison between the proposed 1-π and 2-π scalable model is made, focusing on the following aspects: (1) the complexity of equivalent circuit

* Project supported by the Scientific and Technologic Cooperation Foundation of Yangtze River Delta Area of China (Nos. 2008C16017, 08515810103) and the Major Science and Technology Project of China (No. 2009ZX02303-05).
† Corresponding author. Email: zhh_415@163.com
Received 14 September 2009, revised manuscript received 7 January 2010

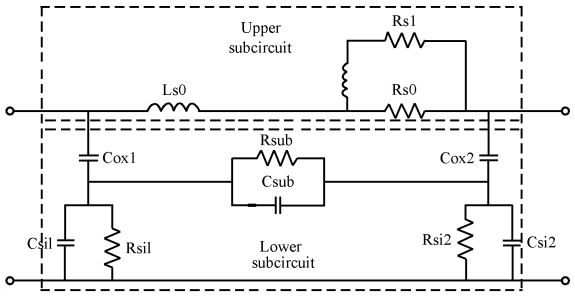

Fig. 1. Enhanced 1-π circuit model.

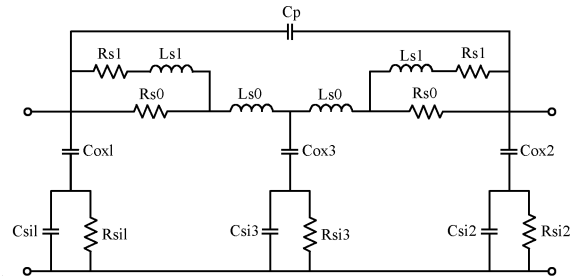

Fig. 2. 2-π circuit model.

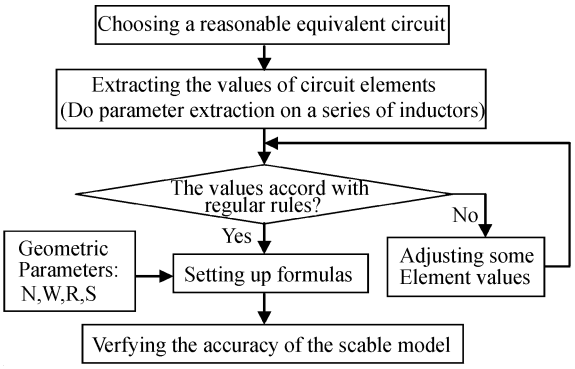

Fig. 3. Procedure of setting up a scalable model.

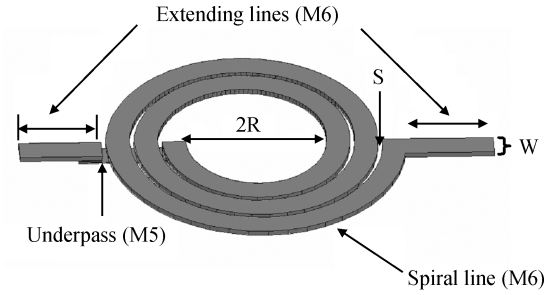

Fig. 4. Structure of spiral inductor.

models, parameter-extraction procedures and scalable rules; (2) the accuracy of the scalable models.

2. Equivalent circuits and parameter extraction

2.1. Enhanced 1-π model

The equivalent circuit for the enhanced 1-π model is shown in Fig. 1.

L_{s0} and R_{s0} are used to model series inductance and resistance. The series branches L_{s1} and R_{s1} in parallel with R_{s0} are used to model wire skin and proximity effects at high frequencies. C_{ox}, C_{si} and R_{si} represent the metalcoxide capacitance, substrate capacitance and resistance, respectively. The parallel networks R_{sub} and C_{sub} are utilized to model the lateral substrate coupling. Based on the initial values of the equivalent-circuit parameters according to the methodology presented in Ref. [13], a set of reasonable values in accordance with physical meanings will be found below through optimization.

2.2. 2-π model

The equivalent circuit for the 2-π model is shown in Fig. 2.The physical meanings of L_{s0}, R_{s0}, L_{s1}, R_{s1}, C_{ox}, C_{si} and R_{si} are the same as in the 1-π model. C_p represents the capacitance between metal spirals and the underpass. The initial values of the elements in this equivalent circuit can be calculated according to the functions presented in Ref. [10]. Then tune C_p, C_{ox3}, C_{si3} and R_{si3} to make L_{eff} and R_{eff} fit well before SRF. Tune C_{ox1}, C_{si1} and R_{si1} to make Q_{11} and L_{11} fit well, and tune C_{ox2}, C_{si2} and R_{si2} to make Q_{22} and L_{22} fit well. The definitions of Q_{11}, Q_{22}, L_{11}, L_{22}, L_{eff} and R_{eff} are the same as in Ref. [10].

3. Scalable model

In this section, the procedure of constructing a scalable model will be introduced. The main steps of setting up a scalable model are shown in Fig. 3.

First, the topology and a series of inductors with regular layout parameters should be chosen; the scalable model will be constructed based on them. Then, the parameter-extraction procedure should be performed on each inductor. After the values of equivalent-circuit elements are extracted from these inductors, it should be examined whether the values accord with the rules based on physical insights. Then readjust the element values that deviate from the physics-based rules. The specific devices whose parameters are unreasonable must be chosen, and then the values must be retuned, making all the parameters satisfy the rules. Finally, the scalable functions that are related to the geometric parameters can be established.

In order to construct the scalable models and verify the accuracy, test structures of circular spiral inductors with various geometrical configurations were fabricated using 0.18-μm 1P6M RF CMOS technology. In this process, the inductor's spiral and extending lines in two ports are made of M6, while M5 is used for the underpass. The thicknesses of M6 and M5 are 2.17 and 0.53 μm, respectively. The sheet resistances of M6 and M5 are 0.0145 and 0.078 $\Omega/\square$, respectively. The dielectric constant and the resistivity of the substrate are 11.9 and 10 Ω·cm. The structure of the circular inductor is shown in Fig. 4.

The two-port S-parameters are measured by an Agilent PNA E8363B network analyzer and Cascade Microtech coplanar GSG probes. The measured two-port S-parameters of the inductor are de-embedded with "open" dummy devices to remove the parasitic effects of probe pads.

Table 1. Layout parameters of the 15 inductors.

DUT# (device under test)	R (μm)	W (μm)	S (μm)	N
D1, 2, …, 5	30	10	2	2.5, 3.5, …, 6.5
D6, 7, …, 10	60	10	2	2.5, 3.5, …, 6.5
D11,12, …, 15	90	10	2	2.5, 3.5, …, 6.5

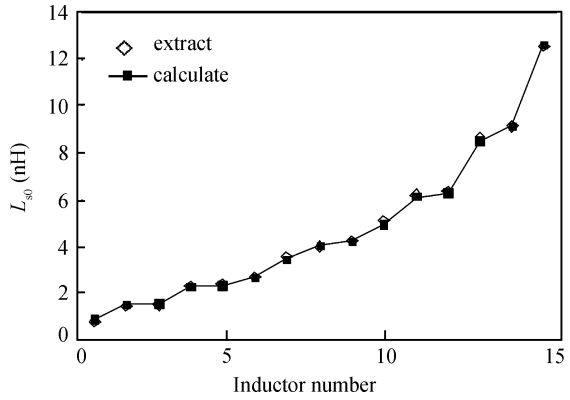

Fig. 5. Comparison of extracted and calculated L_{s0}.

In this experiment, there are 15 spiral inductors fabricated and the layout parameters are outlined in Table 1.

3.1. 1-π scalable model

Next, the procedure of setting up the enhanced 1-π scalable model will be introduced.

3.1.1. L_{s0}

The series inductance L_{s0} includes the inductance of the spirals (L_{s0_spiral}) and the self-inductance of the extending lines (L_{s0_extend}). L_{s0_spiral} and L_{s0_extend} are calculated according to the equation for multiple-turn inductors in Ref. [15] and the function for DC inductance in Ref. [16], respectively. The coefficients β and α_1–α_5 should be further adjusted to achieve an optimal fit between the extracted values and scalable functions.

$$L_{s0\_spiral} = \beta d_{out}^{\alpha_1} W^{\alpha_2} d_{avg}^{\alpha_3} N^{\alpha_4} S^{\alpha_5}, \quad (1)$$

where W, S, d_{out} and d_{avg} in m, and L_{s0_spiral} in H.

$$L_{s0\_extend} = 2l_3\left[\ln\frac{2l_3}{W+t} + 0.50049 + \frac{W+t}{2l_3}\right], \quad (2)$$

where l_3 is the total length of extending lines in cm, W, t metal width and thickness in cm, and L_{s0_extend} in nH.

Therefore,

$$L_{s0} = L_{s0\_spiral} + L_{s0\_extend}. \quad (3)$$

The values of L_{s0} extracted and calculated from the scalable equations (1)–(3) are depicted in Fig. 5.

3.1.2. R_{s0}

The impedance of the upper sub-circuit in Fig. 1 is:

$$R(\omega) = R_{s0}\frac{R_{s1}(R_{s0}+R_{s1}) + \omega^2 L_{s1}^2}{(R_{s0}+R_{s1})^2 + \omega^2 L_{s1}^2}. \quad (4)$$

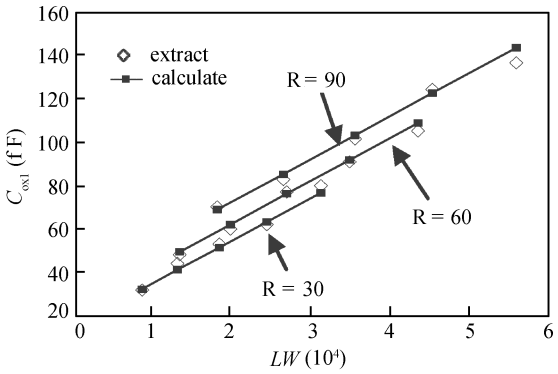

Fig. 6. Comparison of extracted and calculated C_{ox1}.

From Eq. (4), $R_{dc} = R(\omega)$ at $\omega = 0$, hence,

$$R_{dc} = R_{s0}\frac{R_{s1}}{R_{s0}+R_{s1}}. \quad (5)$$

Equation (5) illustrates that the value of R_{dc} is less than R_{s0}. To represent R_{s0}, the sheet resistance of M6 and M5 can first be used to calculate the DC resistance R_{dc}, and then a polynomial is added to fit the deviation of R_{s0} and R_{dc}. Hence,

$$R_{s0} = \frac{l_1+l_3}{W}r_6 + \frac{l_2}{W}r_5 + \left(c_1R^2 + c_2R + c_3\right)NR, \quad (6)$$

where l_1, l_2 the length of spirals and underpass in μm, R the inner radius in μm, and r_5, r_6 the sheet resistance of underpass and spiral.

3.1.3. L_{s1} and R_{s1}

L_{s1} and $R_{s1}$are in proportion to L_{s0} and R_{s0}, respectively. In other papers, the proportional coefficients are constants. The extracted values of L_{s1} and R_{s1} from a series of inductors indicate that a fixed proportional coefficient is not applicable to all the inductors with different geometric sizes. Therefore, polynomial expressions related to geometric parameters are introduced.

$$L_{s1} = \left[\left(b_1R^2 + b_2R + b_3\right)N + b_4R^2 + b_5R + b_6\right]L_{s0}, \quad (7)$$

$$R_{s1} = \left(c_4R^2 + c_5R + c_6\right)R_{s0}. \quad (8)$$

3.1.4. C_{ox1} and C_{ox2}

According to Ref. [5], C_{ox1} and C_{ox2} are in proportion to the area of metal lines. From the extracted values, it is observed that for the inductors with the same inner radius, they are linear with LW. Then the slopes and intercepts are fitted using polynomials in the variable R. Their expressions are as follows:

$$C_{ox1,2} = d_{1,5}LW + d_{2,6}R^2 + d_{3,7}R + d_{4,8}, \quad (9)$$

where $LW = (l_1 + l_3)W$.

The values of C_{ox1} extracted and calculated from the scalable equation (9) are depicted in Fig. 6.

3.1.5. C_{si1}, C_{si2}, R_{si1} and R_{si2}

C_{si1},C_{si2}, R_{si1} and R_{si2} are also linear functions with LW.

$$R_{si1,2} = e_{1,3}LW + e_{2,4}, \quad (10)$$

$$C_{si1,2} = f_{1,3}LW + f_{2,4}. \quad (11)$$

The values of C_{si2} extracted and calculated from the scalable equation (11) are depicted in Fig. 7.

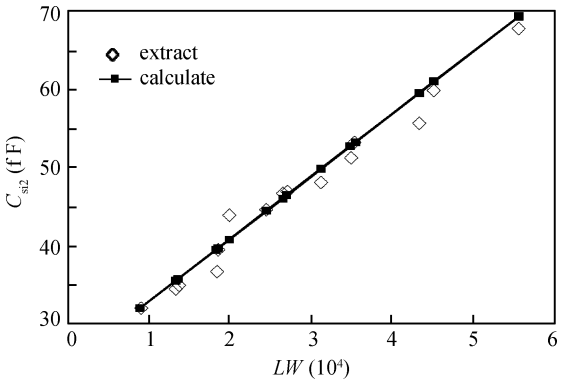

Fig. 7. Comparison of extracted and calculated C_{si2}.

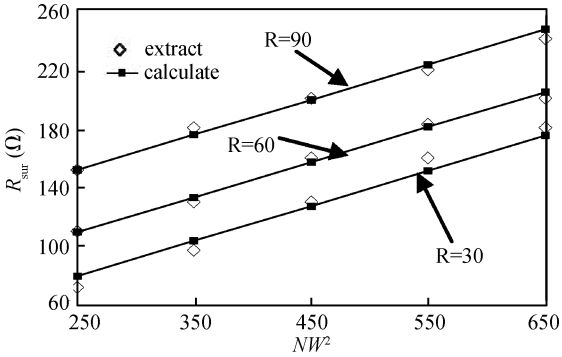

Fig. 8. Comparison of extracted and calculated R_{sub}.

3.1.6. C_{sub} and R_{sub}

The capacitances between metal windings and underpass are represented by C_{sub}. According to the function of C_s in Ref. [5], C_s is in proportion to NW^2. From the extracted values, it is observed that for the inductors with the same inner radius, the values of R_{sub} and C_{sub} are linear with NW^2. Then the slopes and intercepts are fitted using polynomials in the variable R. Therefore, R_{sub} and C_{sub} can be expressed as follows:

$$R_{sub} = g_1 NW^2 + g_2 R^2 + g_3 R + g_4, \tag{12}$$

$$C_{sub} = g_5 NW^2 + g_6 R^2 + g_7 R + g_8. \tag{13}$$

The values of R_{sub} extracted and calculated from the scalable equation (12) are depicted in Fig. 8.

Some of the model coefficients in 1-π scalable rules are presented in Table 2. The values of these model parameters are determined through curve fitting and global optimization.

3.2. 2-π scalable model

The 2-π scalable model is developed in a similar way to the 1-π model. In the 2-π model, the series resistance and inductance are divided into two parts, which makes the values of L_{s0}, R_{s0}, L_{s1} and R_{s1} half of those in the 1-π model. The scalable rules of other equivalent-circuit elements are similar to those of the 1-π model. The scalable equations are as follows:

$$C_{ox1,2,3} = e_{11,15,19} LW + e_{12,16,20} R^2 + e_{13,17,21} R + e_{14,18,22}, \tag{14}$$

Table 2. Model parameters for the 1-π scalable model.

Parameter	Value
β	1.2×10^{-6}
α_1	-1.208
α_2	-0.163
α_3	2.437
α_4	1.8
α_5	-0.049
c_1	1.222×10^{-6}
c_2	-3.5×10^{-4}
c_3	0.0246
c_4	3.758×10^{-4}
c_5	-2.327×10^{-3}
c_6	1.2098
d_1	0.002
d_2	0.00119
d_3	0.1567
d_4	8.4659
e_1	-0.007
e_2	506.423
f_1	0.0002
f_2	10.8721
g_1	0.2375
g_2	0.007121
g_3	0.3459
g_4	3.4825

$$R_{si1,2,3} = \left(f_{11,17,23} R^2 + f_{12,18,24} \cdot R + f_{13,19,25}\right) LW + f_{14,20,26} R^2 + f_{15,21,27} R + f_{16,22,28}, \tag{15}$$

$$C_{si1,2,3} = g_{11,15,19} LW + g_{12,16,20} R^2 + g_{13,17,21} R + g_{14,18,22}, \tag{16}$$

$$C_p = \left(h_{11} R^2 + h_{12} R + h_{13}\right) NW^2 + h_{14} R^2 + h_{15} R + h_{16}. \tag{17}$$

Some of the model coefficients of 2-π scalable rules are listed in Table 3.

The two scalable models are constructed with similar scalable rules which are physics-based and composed of polynomials, facilitating parameter fitting and minimizing the errors. The shape of the inductors in our experiment is circular, but this method is also applicable to inductors with other shapes and fabrication technologies by fitting a new set of model coefficients.

4. Comparison of 1-π and 2-π scalable models

In RF on-chip spiral inductor modeling, 1-π and 2-π models are widely used. When constructing an inductor model library, finding a reasonable topology becomes a critical problem. Making a comparison between 1-π and 2-π scalable models might be helpful in topology selection. Furthermore, among the papers related to the comparison of 1-π and 2-π models, most attention has been paid to fixed models rather than scalable models. Thus, this comparison is made in this paper, focusing on the following aspects: (1) model topologies; (2) the complexity of parameter-extraction procedures and scalable rules; and (3) the accuracy of the scalable models.

Table 3. Model parameters for the 2-π scalable model.

Parameter	Value
e_{11}	0.0013
e_{12}	2.938×10^{-3}
e_{13}	0.0555
e_{14}	2.4054
f_{11}	-3.167×10^{-6}
f_{12}	5.45×10^{-4}
f_{13}	-0.0285
f_{14}	0.0714
f_{15}	-12.544
f_{16}	1329.18
g_{11}	0.0013
g_{12}	4.094×10^{-3}
g_{13}	-0.2379
g_{14}	11.2438
h_{11}	-3.556×10^{-6}
h_{12}	5.367×10^{-4}
h_{13}	0.0072
h_{14}	6.517×10^{-4}
h_{15}	0.02085
h_{16}	4.148

4.1. Model topologies

With the increase of element numbers, the circuit topology of the 2-π model is more complicated than the 1-π model. The conventional 1-π model fails in capturing the distributed effects in two-port Y-parameter measurement. By introducing a central grounded capacitive path (C_{ox3}, C_{si3} and R_{si3}) which can not be shorted by terminal shunt, the distributed effects can not be neglected in 2-π model. This effect is also preserved by the enhanced 1-π model through the parallel network (R_{sub}//C_{sub}).

The two-port effective resistance R_{eff} should be treated carefully while judging the accuracy of an equivalent circuit model. The measured results show that it is equal to the dc resistance first, and then rises with frequency due to skin and proximity effects. After reaching to the maximum, it drops with frequency until achieving a negative value. Similar to the 2-π model, the enhanced 1-π model also has the capability of modeling R_{eff} accurately. The results of R_{eff} modeled by the 2-π and enhanced 1-π models are shown in Fig. 9. It is concluded that the two models both show high accuracy in modeling R_{eff} before SRF.

4.2. Complexity of parameter extraction procedures and scalable rules

The difficulties in extracting parameters and setting up scalable rules rise due to the increase in element numbers. In order to achieve high accuracy on each inductor, optimization should be done. Several parameters sets that can model a single inductor precisely will occur during the optimization, which causes the multi-value problem. In the 2-π model, the phenomenon of multiple solutions will become more serious. Non-optimal solutions will not exhibit physically meaningful scaling characteristics. Thus, how to choose a set of reasonable parameters becomes a difficult problem.

The scalable rules are a series of formulas related to geometric parameters. Errors will be introduced due to the deviation of extracted values and those calculated from the equations. The sources of errors will also increase with the circuit element numbers. Therefore, in the 2-π model, it is harder to find suitable rules for the circuit elements, which makes the inductor models the global optimum.

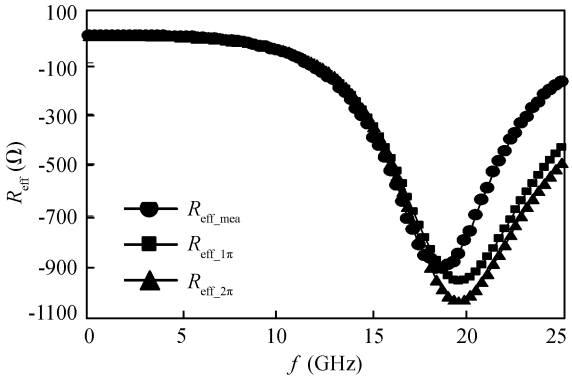

Fig. 9. R_{eff} modeled by enhanced 1-π and 2-π models.

According to the scalable models presented in section 3, it can be observed that there are more model coefficients in the 2-π model. Thus, 2-π model extraction and fitting are more time consuming.

4.3. Accuracy of the scalable models

To validate the model accuracy, the simulated data are compared with measured data considering these important inductor characteristics, such as S-parameter, Y-parameter, Q, L, and R with the frequency ranging from dc to SRF. In this paper, five inductors are chosen as samples to verify the accuracy of two scalable models.

The fitting errors of the Y-parameter are listed in Table 4. For each device, four Y-parameter fitting errors are separated with a real part and an imaginary part.

The definitions of fitting errors are as follows:

$$\mathrm{Re}(Y_{\mathrm{param}})\_\mathrm{error}(\%) = \sqrt{\left(\frac{1}{n}\sum_{1}^{n}\frac{|\mathrm{real}(Y_{\mathrm{xy,mea}}) - \mathrm{real}(Y_{\mathrm{xy,sim}})|^2}{\left(\sum_{1}^{n}|\mathrm{real}(Y_{\mathrm{xy,mea}})|^2/n\right)}\right)} \times 100,$$

$$\mathrm{Im}(Y_{\mathrm{param}})\_\mathrm{error}(\%) = \sqrt{\left(\frac{1}{n}\sum_{1}^{n}\frac{|\mathrm{imag}(Y_{\mathrm{xy,mea}}) - \mathrm{imag}(Y_{\mathrm{xy,sim}})|^2}{\left(\sum_{1}^{n}|\mathrm{imag}(Y_{\mathrm{xy,mea}})|^2/n\right)}\right)} \times 100,$$

where n is the number of frequency points.

From the comparison of the Y-parameter in Table 4, it can be concluded that the two models both show high accuracy. Also, the error of the 2-π model is just a bit lower than the 1-π model. The same comparisons have been done for the S-parameter, and good coincidence between the simulated and measured S-parameter has also been achieved.

The results of Q, L and R are plotted in Fig. 10–12 and their RMS errors are outlined in Table 5.

From Fig.10, it is found that the curves of measured L, 1-π modeled and 2-π modeled L are fitted well, which shows

Table 4. Fitting errors of the Y-parameter.

Parameter		Y_{11} (%)		Y_{12} (%)		Y_{21} (%)		Y_{22} (%)	
		real	imag	real	imag	real	imag	real	imag
D3	1-π	2.6	4.9	2.6	4.8	2.6	4.8	2.6	4.9
	2-π	3.9	2.3	4.0	2.4	4.0	2.3	4.0	2.2
D7	1-π	3.2	0.9	3.3	1.3	3.3	1.3	3.3	1
	2-π	2.7	0.8	2.8	1.2	2.8	1.3	2.7	0.8
D9	1-π	2.5	2.7	2.6	2.7	2.4	2.5	2.4	2.7
	2-π	2	1.7	2.1	1.9	2	1.8	1.9	1.7
D12	1-π	3.2	1.7	3.2	2.0	3.4	2.1	3.3	1.8
	2-π	3.3	2	3.3	2.3	3.5	2.4	3.3	2
D14	1-π	2.8	1.6	2.8	1.7	2.9	1.7	2.8	1.6
	2-π	1.8	1.4	1.9	1.8	2.1	2.0	1.9	1.5

Table 5. RMS errors of Q, L and R.

Parameter	D3 (%)		D7 (%)		D9 (%)		D12 (%)		D14 (%)	
	1-π	2-π	1-π	2-π	1-π	2-π	1-π	2-π	1-π	2-π
Q	6.1	5.3	5.6	12	2.6	8.0	5.9	13	3.1	10
L	1.5	2.3	1.2	1.2	1.9	1.1	2.1	2.0	0.9	2.1
R	6.0	5.6	5.2	11	2.8	8.5	6.1	12	3.5	11.8

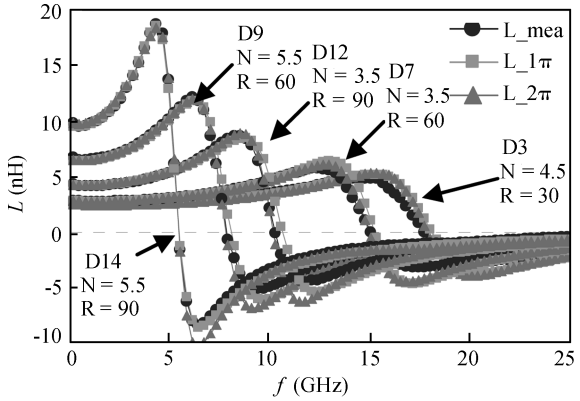

Fig. 10. Comparison of inductances.

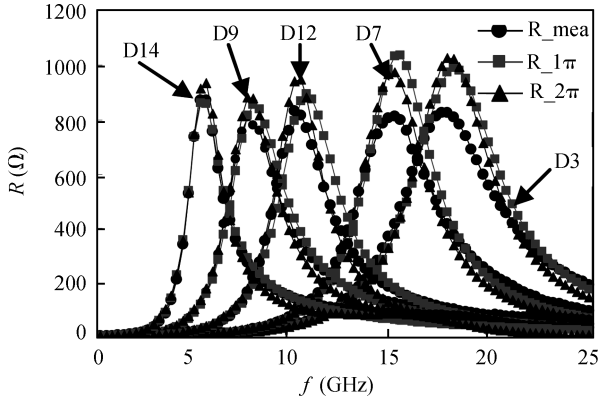

Fig. 12. Comparison of resistances.

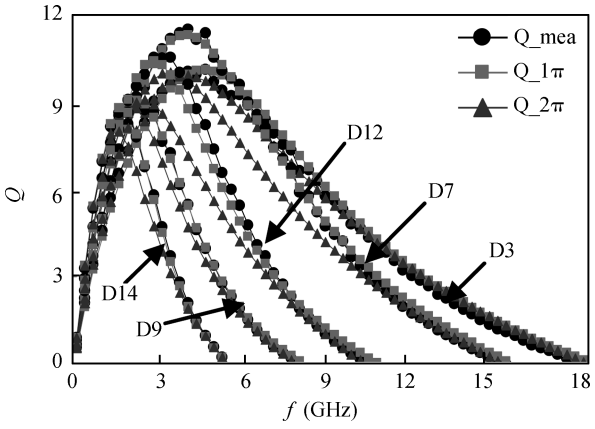

Fig. 11. Comparison of quality factors.

that high accuracy is achieved by the two models in modeling inductance. The result is also proved by the RMS errors listed in Table 5.

Figure 11 shows that the measured Q and 1-π modeled Q are fitted well. However, Q of devices D7 and D12 represented by the 2-π model deviates from measured data at the maximum while their Y-parameters are fitted well. Q is calculated through the function Q= Im(1/Y_{11})/Re(1/Y_{11}). The data in Table 4 show that errors of the real and imaginary parts of Y_{11} both exist. One explanation for the phenomenon of Q is that when it is calculated through the above function, the errors of the real and imaginary parts are superimposed. The RMS errors in Table 5 illustrate that the 1-π model has high accuracy in representing Q.

Figure 12 shows that the measurement and simulation for R coincide before the peak value, but errors near the peak value are noticeable, leading to the distinct errors of R in Table 5. The frequency corresponding to the peak value of R is SRF. Beyond SRF, the spiral inductor appears to be capacitive and can no longer be used as an inductor. Moreover, inductors are usually utilized in the frequency band where the inductance changes gently. Thus, the errors are still acceptable.

From the above comparison, it can be concluded that good coincidence between the simulated and measured data have been achieved. In this experiment, the enhanced 1-π model shows higher accuracy in modeling the characteristics of Q, L and R, while the 2-π model is more accurate in modeling the

Y-parameter. Meanwhile, the enhanced 1-π model has advantages over the 2-π model in its simplicities of circuit topology, physical meanings, parameter-extraction procedure and scalable rules. The 1-π model also shows higher stability.

5. Conclusions

Two scalable models based on the enhanced 1-π and 2-π topologies have been proposed. Similar scalable rules are utilized to construct the two scalable models. A comparison between the 1-π and 2-π scalable models has been done. The results show that excellent agreement between measured and simulated data has been achieved. From the experimental results, it can be concluded that the enhanced 1-π model satisfies the demand for accuracy and rapidity in on-chip inductor modeling before SRF. On the other hand, the distributed nature of the metal windings and capacitive coupling are considered in detail in the 2-π model, which enables the 2-π model to achieve a high accuracy in a wider frequency band than the 1-π model.

References

[1] Lin J C H, Ye T H H, Chen C H, et al. State-of-the-art RF/analog foundry technology. Bipolar/BiCMOS Circuit and Technology Meeting, 2002: 73

[2] Cheng Y. An overview of device behavior and modeling of CMOS technology for RFIC design. Electron Devices for Microwave and Optoelectronic Applications, 2003: 109

[3] Iwai H. RF CMOS technology. Radio Science Conference, 2004: 296

[4] Haran B S. 22 nm technology compatible fully functional 0.1 μm^2 6T-SRAM cell. IEDM, 2008: 625

[5] Yue C P, Wong S S. Physical modeling of spiral inductors on silicon. IEEE Trans Electron Devices, 2000, 47: 3

[6] Lai I C H, Fujishima M. A new on-chip substrate-coupled inductor mode implemented with scalable expressions. IEEE J Solid-State Circuits, 2006, 41: 11

[7] Gil J, Shin H. A simple wide-band on-chip inductor model for silicon-based RFICs. IEEE Trans Microw Theory Tech, 2003, 51: 9

[8] Huang F, Lu J, Jiang N, et al. Frequency-independent asymmetric double-π equivalent circuit for on-chip spiral inductors: physics-based modeling and parameter extraction. IEEE J Solid-State Circuits, 2006, 41: 10

[9] Watson A C, Melendy D, Francis P, et al. A comprehensive compact-modeling methodology for spiral inductors in silicon-based RFICs. IEEE Trans Microw Theory Tech, 2004, 52: 3

[10] Gao W, Yu Z. Scalable compact circuit model and synthesis for RF CMOS spiral inductors. IEEE Trans Microw Theory Tech, 2006, 54: 3

[11] Guo J C, Tan T Y. A broadband and scalable model for on-chip inductors incorporating substrate and conductor loss effects. IEEE Trans Electron Devices, 2006, 53: 3

[12] Horng T S, Jau J K, Huang C H, et al. Synthesis of a super broadband model front-chip spiral inductors. IEEE RFIC Symp Dig, 2004: 453

[13] Chen H H, Zhang H W, Chung S J, et al. Accurate systematic model-parameter extraction for on-chip spiral inductors. IEEE Trans Electron Devices, 2008, 55: 11

[14] Kang M, Gil J, Shin H, et al. A simple parameter extraction method of spiral on-chip inductors. IEEE Trans Electron Devices, 2005, 52: 9

[15] Mohan S S, del Mar Hershenson M, Boyd S P, et al. Simple accurate expressions for planar spiral inductances. IEEE J Solid-State Circuits, 1999, 34: 1419

[16] Grover F W. Inductance calculations. New York: Van Nostrand, 1962